Solar Energy Materials & Solar Cells 95 (2011) 1146–1150

Contents lists available at ScienceDirect

Solar Energy Materials & Solar Cells

journal homepage: www.elsevier.com/locate/solmat

Morphological and electrical effect of an ultrathin iridium oxide hole extraction layer on P3HT:PCBM bulk-heterojunction solar cells

Gwan Ho Jung [a,b], Kyung-Geun Lim [a], Tae-Woo Lee [a], Jong-Lam Lee [a,b,*]

[a] Department of Materials Science and Engineering, Pohang University of Science and Technology (POSTECH), Pohang, Gyeongbuk 790-784, Republic of Korea
[b] Graduate Institute of Advanced Materials Science, Pohang University of Science and Technology (POSTECH), Pohang, Gyeongbuk 790-784, Republic of Korea

ARTICLE INFO

Article history:
Received 10 November 2010
Accepted 16 December 2010
Available online 8 January 2011

Keywords:
Organic solar cell
P3HT:PCBM
Hole extraction layer
Iridium oxide
Polymer solar cell

ABSTRACT

An ultrathin iridium layer was treated with O_2-plasma to form an iridium oxide (IrO_x), employed as a hole extraction layer in order to replace poly(3,4-ethylenedioxythiophene):poly(styrene-sulfonate) (PEDOT:PSS) in organic photovoltaic (OPV) cells with poly(3-hexylthiophene):phenyl-C61-butyric acid methyl ester (P3HT:PCBM). The IrO_x layer affects the self-organization of the P3HT:PCBM photo-active layer due to its hydrophobic nature, inducing a well-organized intraplane structure with lamellae oriented normal to the substrate. Synchrotron radiation photoelectron spectroscopy results showed that the work function increased by 0.57 eV as the Ir layer on ITO changed to IrO_x by the O_2-plasma treatment. The OPV cell with IrO_x (2.0 nm) exhibits increased power conversion efficiency as high as 3.5% under 100 mW cm^{-2} illumination with an air mass (AM 1.5G) condition, higher than that of 3.3% with PEDOT:PSS.

1. Introduction

Organic photovoltaics (OPVs) have emerged as promising alternatives to silicon based solar cells due to their advantages in terms of applying low-cost, large-area, and mechanically flexible substrates as well as the possibility of using roll-to-roll fabrication processes [1–8]. OPV cells have been fabricated with an active layer composed of a blend of regio-regular poly(3-hexylthiophene) (P3HT) and the fullerene derivative [6,6]-phenyl-C61 butyric acid methyl ester (PCBM). In bulk-heterojunction (BHJ) OPVs, an important factor in determining the device performance is the charge extraction from the active layer to the electrodes [9,10]. Therefore, the photocurrent depends on the interface between the active layer and electrodes. To obtain good interfacial properties between the active layer and the anode, poly(3,4-ethylenedioxythiophene):poly(styrene-sulfonate) (PEDOT:PSS) is commonly used as a hole extraction layer (HEL) to increase the crystallinity of the subsequent active layer of P3HT as well as to enhance the extraction of holes [11]. However, PEDOT:PSS deposited on indium tin oxide (ITO) anodes is highly acidic (pH 1.3–2.1), resulting in the dissociation of ITO into In and Sn atoms at the surface of the ITO [12]. The In and Sn atoms can then easily migrate into the PEDOT:PSS layer upon thermal annealing [13]. Moreover, in previous works, PEDOT:PSS films formed by spin coating were not uniform micro-structurally or electrically [14,15]. This led to inhomogeneous charge extraction, resulting in "dead zones" in some regions [14]. These issues illustrate the need for a chemically stable and mechanically uniform anode as a HEL to replace PEDOT:PSS for OPVs.

Several kinds of oxide HEL have been proposed to alternate the PEDOT:PSS layer, as some oxides have higher work functions than ITO. When a few nanometers-thick V_2O_5, MoO_3, and NiO were deposited on an ITO anode using either thermal evaporation or pulsed laser deposition [16–18], a slight decrease in the efficiency of the OPV was observed. It was found that the atomic composition of the oxide could change with the deposition rate during thermal evaporation, leading to a nonuniform distribution of the work function across the substrate [18]. Controlling the surface energy before deposition of the P3HT:PCBM active layer is critical to increasing the efficiency of the OPV. The surface energy of the thermal-evaporated oxides was nonuniform over the substrate, because of inconsistent cohesion between the P3HT:PCBM active layer and metal oxide [19]. In order to enhance the uniformity, a self-assembled monolayer (SAM) was employed. The SAM controlled the configuration of P3HT with a preferred orientation of (1 0 0) normal to the substrate, yielding high mobility in P3HT [20,21]. However, molecular sized defects or holes arose in the self-assembled layer, leading to "dead zones" in some regions [21].

Employing an HEL oxide to fulfill both high work function and high dispersive surface energy could provide a means of enhancing the efficiency as well as ensuring the reliability of OPVs. O_2-plasma treatment is effective not only in enhancing the surface energy by converting the thin metal (~2 nm) to a metal oxide but also in increasing the work function via an increase of the oxygen content at the surface of the metal oxide. However, no studies on the implementation of a plasma-induced metal oxide anode, capable of

* Corresponding author at: Department of Materials Science and Engineering, Pohang University of Science and Technology (POSTECH), Pohang, Gyeongbuk 790-784, Korea, Fax: +82 54 279 5242.
E-mail address: jllee@postech.ac.kr (J.-L. Lee).

0927-0248/$ - see front matter © 2010 Elsevier B.V. All rights reserved.
doi:10.1016/j.solmat.2010.12.039

simultaneously increasing both the surface energy and the work function, have been reported to date.

In this study, O_2-plasma treatment was applied to iridium (Ir) in order to produce iridium oxide (IrO_x), used as the HEL to alternate the PEDOT:PSS. IrO_x is a transparent conducting oxide, and the work function of IrO_x (> 5.0 eV) is higher than that of ITO (4.4–4.7 eV) [22]. Moreover, IrO_x has a surface with hydrophobic nature. Thus, it is expected that the HEL of IrO_x between ITO anodes and active layer could improve the extraction of holes. The surface energy of IrO_x HEL was monitored using contact angle measurement. The crystallographic orientation of P3HT stacks on the treated surface was examined using grazing angle X-ray diffraction (GIXRD). Ultraviolet photoelectron spectroscopy (UPS) and X-ray photoemission spectroscopy (XPS) were employed to measure the change in the work function and chemical composition at the surface of IrO_x, respectively [23]. From these results, the effects of the O_2-plasma-induced IrO_x HEL on the power conversion efficiency are discussed.

2. Experimental

Active blend films were fabricated between a transparent anode and a cathode. The anode consisted of a glass substrate coated with indium tin oxide (ITO) and was modified by an O_2-plasma treated Ir thin film layer. The cathode consisted of LiF (ca. 1 nm) coated with Al (ca. 100 nm). Both the Ir and LiF/Al films were deposited at a base pressure of 2×10^{-6} Torr. Glass coated with ITO (150 nm thick, ~15 Ω/sq) was used as the starting substrate. The ITO glass was cleaned using O_2-plasma for 1 min under 100 mTorr with a power of 150 W prior to device fabrication [24,25]. A 2-nm-thick Ir layer was then deposited using an e-beam evaporator. The Ir film was exposed to O_2-plasma for 1 min to form iridium oxide. After O_2-plasma treatment for 1 min, the substrates were transferred to a N_2-filled glove box (< 0.1 ppm O_2 and H_2O). Regio-regular poly (3-hexylthiophene) (P3HT, purchased from Rieke Metals and used as received) was first dissolved in 1,2-dichlorobenzene (DCB) to make a 20 mg/ml solution, followed by blending with phenyl-C61-butyric acid methyl ester (PCBM, Nano-C, used as received) in a 1:1 weight ratio. The blend was stirred for ~14 h in a glove box before being spin-coated (700 rpm, 30 s) on top of the ITO/IrO_x surface. The active layer thickness was measured as ~200 nm by a surface profiler. The devices were annealed on a hot plate in a glove box at 130 °C for 10 min. Six types of OPVs were prepared with PEDOT:PSS and various thickness of the IrO_x layer in a range of 0–2.5 nm. The active device area was ca. 0.04 cm^2. The *J–V* curves were measured under air ambient with glass encapsulation using a Keithley 2400 source measurement unit. The photocurrent was measured under AM 1.5G 100 mW cm^{-2} illumination from an Oriel 150 W solar simulator. The light intensity was determined using a mono-silicon detector calibrated by the National Renewable Energy Laboratory (NREL). For accurate measurement of the device performance, only the active area of the samples was exposed.

3. Results and discussion

Fig. 1(a) presents a schematic diagram illustrating the device structure with the HEL between ITO and the P3HT:PCBM active layer. The effect of the HEL on the P3HT stacks in polymer solar cells is illustrated in Fig. 1(b) and (c). After insertion of the O_2-plasma treated Ir (IrO_x) thin film as a HEL, well organized P3HT stacks with preferred orientation normal to the substrate (see Fig. 1(c)) are observed in comparison with the PEDOT:PSS in Fig. 1(b). The cell structure employs P3HT as a donor and PCBM as an acceptor material with the relevant energy levels shown in Fig. 1(d). As noted above, IrO_x was chosen as the p-type HEL. The fermi energy level (EF) of IrO_x aligns

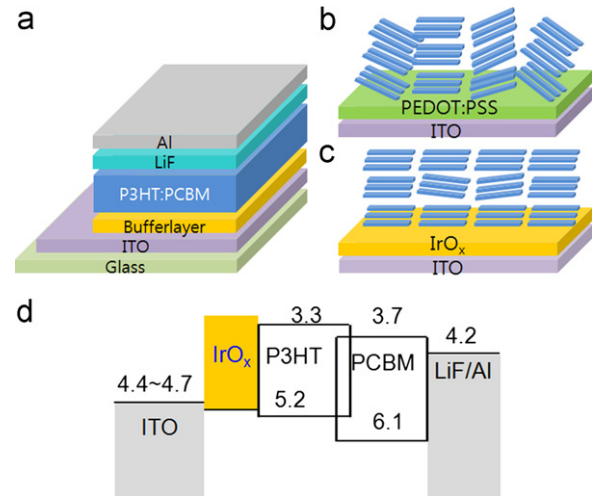

Fig. 1. (a) Schematic device structure of polymer solar cells in this study. Schematic illustration of P3HT stacks on (b) ITO and (c) IrO_x HEL. (d) Schematic band diagram of device components referenced to the vacuum level.

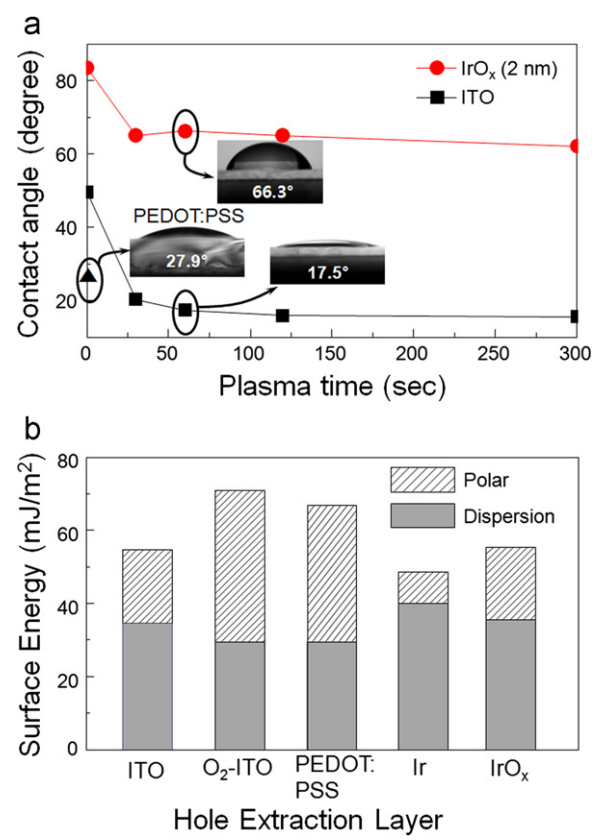

Fig. 2. (a) Contact angle of ITO and IrO_x coated ITO as a function of O_2-plasma treatment time, and (b) surface energy distribution with ITO and Ir-coated ITO before and after O_2-plasma for 60 s.

on top of the ITO surface, close to the highest occupied molecular orbital (HOMO) of the PCBM. Additional discussion of the energy level alignment is presented below.

To investigate the effect of the surface energy for the HEL, the surface energy of ITO and Ir (2 nm) thin film was measured using the contact angle of distilled (DI) water as a function of plasma time, as shown in Fig. 2. The contact angle of DI water on PEDOT:PSS is 27.9°. In addition, the contact angle decreases from 49.5° to 17.5°

for ITO and from 83.6° to 66.3° for the Ir thin film after O_2-plasma treatment for 60 s. No significant difference of contact angle between on PEDOT:PSS and on O_2-plasma treated ITO was observed. The contact angle of DI water on PEDOT:PSS and O_2-plasma treated Ir and ITO is shown in the inset of Fig. 2(a). Note that the contact angle of the Ir thin film still remains above 60° even after oxygen plasma treatment for 300 s. The surface energies of the IrO_x film and ITO substrates were determined from the contact angle using DI water and diiodomethane as probe liquids. Moreover, the surface energy was calculated using the geometric mean equation,

$$(1+\cos\theta)\gamma_{pl} = 2(\gamma_s^d\gamma_{pl}^d)^{1/2} + 2(\gamma_s^p\gamma_{pl}^p)^{1/2}$$

where γ_s and γ_{pl} are the surface energies of the sample and the probe liquid, respectively, and the superscripts d and p refer to the dispersion and polar (nondispersion) components of the surface energy, respectively. The total surface energy for both ITO and Ir films coated ITO increased after O_2-plasma treatment. The polar component of the surface energy in ITO substantially increased from 20.1 to 41.5 mJ/m^2 after O_2-plasma treatment, but that of the Ir (2 nm) film only slightly increased from 8.6 to 19.9 mJ/m^2. The dispersive component of the surface energy for both ITO and Ir-coated ITO decreased from 34.5 and 40 mJ/m^2 to 29.4 and 35.5 mJ/m^2, respectively. The calculated surface energy of O_2-plasma treated ITO is similar to PEDOT:PSS. In IrO_x coated ITO, the dispersive energy is higher than that of ITO, PEDOT:PSS and the polar component, thus indicating that a hydrophobic surface property was maintained after O_2-plasma; this is beneficial for ordered P3HT stacks with preferred orientation of (1 0 0) in a direction normal to the substrate [20].

Fig. 3 displays the two-dimensional (2D) grazing incident X-ray diffraction (GIXRD) results obtained using a synchrotron X-ray beam (4CII beamline, Pohang Light Source) from P3HT:PCBM blend films on ITO, PEDOT:PSS and IrO_x coated ITO glass substrates before and after thermal annealing at 130 °C for 10 min. To investigate the effect of surface energy on the structure of the P3HT:PCBM layer, measurements were carried out using GIXRD. The wavelength of the X-ray was 1.3807 Å and the incident angle was fixed at 0.18°. The (1 0 0), (2 0 0), and (3 0 0) diffraction patterns are the main peaks in the out-of-plane (OOP) directions and this trend is more pronounced after annealing. These OOP diffraction patterns indicate that all P3HT:PCBM blend films show a well-organized intraplane structure with lamellae oriented normal to the substrate. In comparison to the IrO_x HEL sample, the ITO and PEDOT:PSS sample show some arcing with the (1 0 0) direction after annealing in Fig. 3(d) and (e), indicating that the P3HT stacks are less well oriented in this sample.

Fig. 4 represents the work function measured using secondary-electron emission spectra (4BI beamline, Pohang Light Source) for ITO, PEDOT:PSS, and IrO_x HEL to analyze the energy level alignment. The work function of pre-cleaned ITO was measured to be 4.43 eV at He I excitation of 21.2 eV as a UV energy source. When Ir was treated by O_2-plasma, the work function of IrO_x coated ITO increased to 5.0 eV, consistent with the measured work function of PEDOT:PSS (4.95 eV). This increase in the work function of Ir is due to Ir-oxide formed by O_2-plasma. Fig. 4(b) shows Ir 4*f* SRPES core-level spectra for the Ir layer. The peaks corresponding to Ir–Ir bonds decreased and new peaks appeared at higher binding energies in the O_2-plasma treated samples. Since the binding energies of the new peaks were 0.9 eV higher than those of Ir–Ir bonds, they were determined to be Ir–O bonds [26]. The escape depth (λ) of the Ir 4*f*

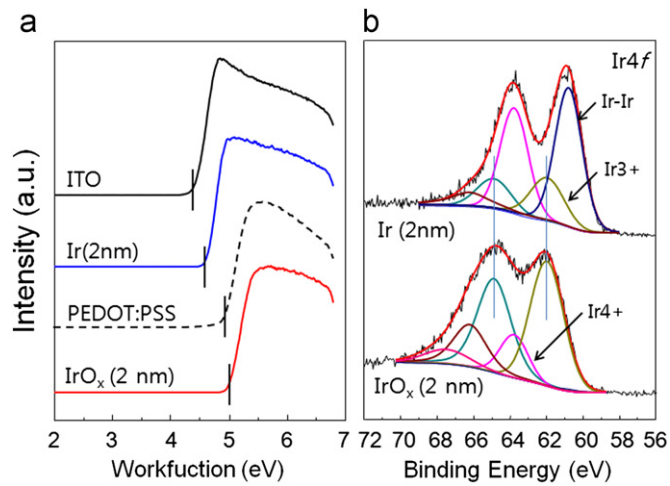

Fig. 4. (a) Secondary-electron emission spectra of ITO, Ir, PEDOT:PSS, and IrO_x. (b) Ir 4*f* core-level spectra of Ir before and after O_2-plasma.

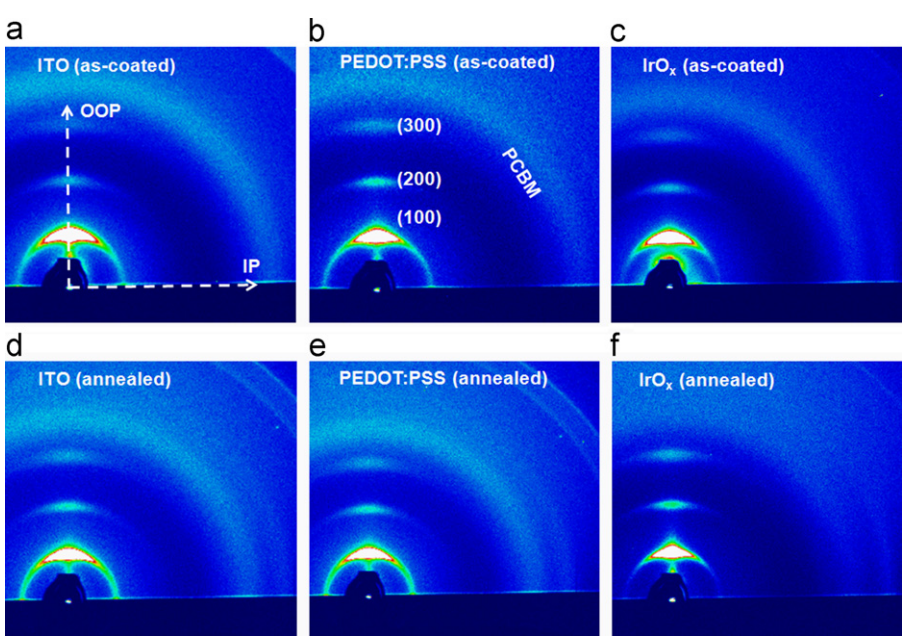

Fig. 3. Two-dimensional GIXRD results for P3HT:PCBM (1:1) blend films of (a) not-annealed on ITO, (b) annealed on ITO, (c) not-annealed on IrO_x coated ITO, and (d) annealed on IrO_x coated ITO.

photoelectron is calculated using the empirical equation [27], $\lambda = 0.41a^{0.5}E^{0.5}$, where a is the radius of the atom (0.136 nm for Ir) and E is the electron kinetic energy (in eV). Based on the empirical equation, λ is calculated to be 3.7 nm for Ir. The escape depth of the Ir 4*f* photoelectron (3.7 nm) is larger than that of the IrO_x film thickness (2.5 nm) used in the experiment. These confirm that the Ir film was completely transformed to Ir-oxide by the O_2-plasma treatment.

The transmittance of the PEDOT:PSS and IrO_x coated ITO glass substrates is shown in Fig. 5. In all cases, the substrates were illuminated from the glass side, as shown in the inset. The transmittance decreased when the thickness of IrO_x increased from 1.3 to 2.5 nm. In general, metal oxides have a high band gap, leading to the high optical transmittance in the visible range. In the meanwhile, the iridium dioxide has a blue-black color due to intraband electronic transitions within the Ir t_{2g} band [28,29]. When it becomes thick, the absorption could increase because of the increase of intraband transition. Therefore, the transmittance of 2.5-nm-thick IrO_x is lower than that of PEDOT:PSS and 1.3-nm-thick iridium oxide. Slightly different photon flux is incident on the photo-active layer in all devices between PEDOT:PSS and IrO_x HELs, but not significant. This would result in a slightly low J_{sc} in the case of an IrO_x interlayer solar cell as compared to PEDOT:PSS. The highest transmittance of the IrO_x HEL of 1.3 nm thickness was measured to be 87%, averaged from 300 to 800 nm wavelength. However, the efficiency of 1.3 nm thickness IrO_x was slightly lower than that of the 1.6 nm thickness case, as seen in Table 1, as the former does not cover the ITO surface uniformly.

Fig. 6 shows typical *J–V* curves of devices with no HEL, PEDOT:PSS, and a 2 nm thick IrO_x layer, respectively. Devices fabricated on bare ITO consistently exhibit low open circuit voltage (V_{oc}) and low power conversion efficiency (PCE) responses. In the plot, V_{oc}=0.530 V, short circuit current (J_{sc})=8.3 mA/cm^2, FF=15.7%, and PCE=0.7% for a device fabricated on bare, clean ITO. In contrast, introduction of the IrO_x interlayer substantially increases the response metrics. The IrO_x-based device in Fig. 2 exhibits V_{oc}=0.573 V, J_{sc}=8.6 mA/cm^2, FF=71.2%, and PCE=3.5%, comparable to PEDOT:PSS devices fabricated in parallel; for PEDOT:PSS, V_{oc}=0.593 V, J_{sc}=9.4 mA/cm^2, FF=58.8%, and PCE=3.27%. The solar cell performances of all devices discussed in this study are summarized in Table 1. Compared to the device without the IrO_x HEL, the device with IrO_x HEL showed a significantly improved fill factor (FF). The enhanced FF provides evidence of an improved transport property, which could be attributed to more facile charge extraction due to the increased crystallinity of the P3HT stacks with lower hole barrier height [17,30].

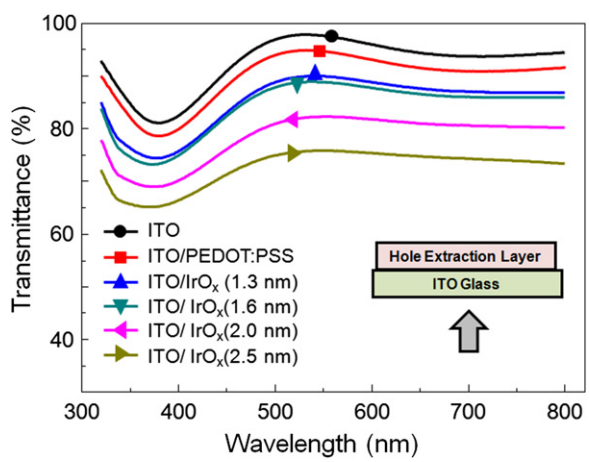

Fig. 5. Transmittance of ITO glass coated with thin films of PEDOT:PSS (25 nm) and oxygen plasma treated on Ir thin film for 1 min with various thicknesses. Inset: schematic diagram of direction of incident light to the IrO_x coated ITO substrate.

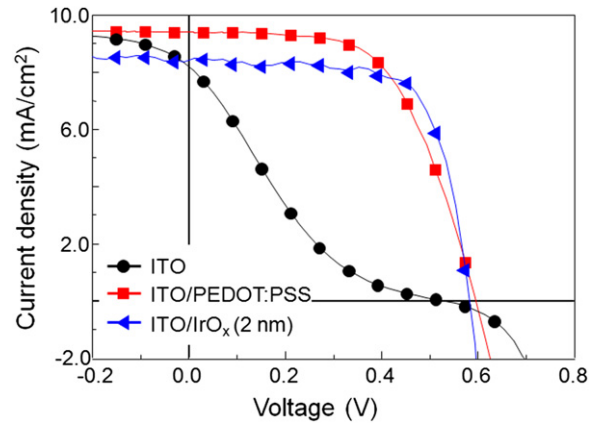

Fig. 6. *J–V* curves for polymer solar cells with and without IrO_x HEL. The reference device has the structure: glass/PEDOT:PSS/ITO/P3HT:PCBM/LiF/Al.

Table 1
Photovoltaic performances of the devices with and without various thickness IrO_x HEL on an ITO glass substrate, fabricated 4 times. The light condition was AM 1.5G 100 mWcm^{-2} illumination for the measurements.

HEL	HEL thickness (nm)	V_{oc} (V)	J_{sc} (mA/cm^2)	FF (%)	PCE (%)
PEDOT:PSS	30	0.593	9.4	58.8 ± 0.4	3.3 ± 0.02
No		0.533 ± 0.04	8.3 ± 0.4	15.7 ± 2	0.7 ± 0.20
IrO_x	1.3	0.573 ± 0.01	7.8 ± 0.2	57.8 ± 1.2	3.0 ± 0.02
	1.6	0.573 ± 0.01	8.6 ± 0.1	71.2 ± 0.8	3.5 ± 0.01
	2.0	0.573 ± 0.01	8.4 ± 0.1	72.4 ± 0.2	3.5 ± 0.02
	2.5	0.573 ± 0.01	7.5 ± 0.1	70.0 ± 0.3	3.0 ± 0.05

4. Conclusions

A fabricated HEL with high dispersive surface energy and a high work function in polymer solar cells showed improved performance. Insertion of an IrO_x HEL at the anode of the ITO/organic interface significantly improved the J_{sc} (from 8.3 to 8.6 mA/cm^2), V_{oc} (from 0.53 to 0.57 V), and PCE (from 0.7 to 3.5%) of a BHJ OPV compared with a control device of ITO without the HEL. The IrO_x HEL induced well-ordered P3HT stacks with a preferred orientation of (1 0 0) normal to the substrate and a high work function of 5.0 eV lowered the hole extraction barrier. The increased crystallinity and lowered hole barrier with insertion of the IrO_x HEL induced higher FF than that of device with PEDOT:PSS HEL. Chemically stable IrO_x enabling easy device fabrication could therefore be used as an alternative material for PEDOT:PSS and is applicable to general anode HELs on organic electronics.

Acknowledgements

This work was supported in part by Priority Research Centers Program through the National Research Foundation of Korea (NRF) funded by the Ministry of Education, Science and Technology (2010-0029711), in part by Basic Science Research Program through the National Research Foundation of Korea(NRF) funded by the Ministry of Education, Science and Technology (2010-0012919), and in part by WCU (World Class University) program through the Korea Science and Engineering Foundation funded by the Ministry of Education, Science and Technology (Project No. R31-2008-000-10059-0).

References

[1] W. Cai, X. Gong, Y. Cao, Polymer solar cells: recent development and possible routes for improvement in the performance, Sol. Energy Mater. Sol. Cells 94 (2010) 114–127.

[2] T.-W. Lee, K.-G. Lim, D.-H. Kim, Approaches toward efficient and stable electron extraction contact in organic photovoltaic cells: inspiration from the organic light-emitting diodes, Electron. Mater. Lett. 6 (2010) 41–50.

[3] G. Li, V. Shrotriya, J. Huang, Y. Yao, T. Motiarty, K. Emergy, Y. Yang, High-efficiency solution processable polymer photovoltaic cells by self-organization of polymer blends, Nat. Mater. 4 (2005) 864–868.

[4] F.C. Krebs, S.A. Gevorgyan, J. Alstrup, A roll-to-roll process to flexible polymer solar cells: model studies, manufacture and operational stability studies, J. Mater. Chem. 19 (2009) 5442–5451.

[5] S.Y. Kim, K. Kim, K. Hong, J.-L. Lee, Investigation of metal peel-off technique for the fabrication of flexible organic light emitting diodes, J. Electrochem. Soc. 156 (2009) J253–J257.

[6] F.C. Krebs, J. Fyenbo, M. Jorgensen, Product integration of compact roll-to-roll processed polymer solar cell modules: methods and manufacture using flexographic printing, slot-die coating and rotary screen printing, J. Mater. Chem. 20 (2010) 8994–9001.

[7] F.C. Krebs, T. Tromholt, M. Jorgensen, Upscaling of polymer solar cell fabricated fabricated using full roll-to-roll processing, Nanoscale 2 (2010) 873–886.

[8] F.C. Krebs, T.D. Nielsen, J. Fyenbo, M. Wadstrom, M.S. Pedersen, Manufacture, integration and demonstration of polymer solar cells in a lamp for the "Lighting Africa" initiative, Energy Environ. Sci. 3 (2010) 512–525.

[9] S. Gunes, H. Neugebauer, N.S. Sariciftci, Conjugated polymer-based organic solar cells, Chem. Rev. 107 (2007) 1324–1338.

[10] P. Vanlaeke, A. Swinnen, I. Haeldermans, G. Vanhoyland, T. Aernouts, D. Cheyns, C. Deibel, J. D'Haen, P. Heremans, J. Poortmans, J.V. Manc, P3HT/PCBM bulk heterojunction solar cells: relation between morphology and eletro-optical characteristics, Sol. Energy Mater. Sol. Cells 90 (2006) 2150–2158.

[11] Y. Kim, A.M. Ballantyne, J. Nelson, D.D.C. Bradley, Effects of thickness and thermal annealing of the PEDOT:PSS layer on the performance of polymer solar cells, Org. Electron. 10 (2009) 205–209.

[12] T.-W. Lee, Y. Chung, Control of the surface composition of a conducting-polymer complex film to tune the work function, Adv. Func. Mater. 18 (2008) 2246–2252.

[13] T.-W. Lee, Y. Chung, O. Kwon, J.-J. Park, Self-organized gradient hole injection to improve the performance of polymer electroluminescent devices, Adv. Func. Mater. 17 (2007) 390–396.

[14] A.W. Hains, T.J. Marks, High-efficiency hole extraction/electron-blocking layer to replace poly(3,4-ethylenedioxythiophene):poly(styrene sulfonate) in bulk-heterojunction polymer solar cells, Appl. Phys. Lett. 92 (2008) 0235041–0235043.

[15] M. Kemerink, S. Timpanaro, M.M. de Kok, E.A. Meulenkamp, F.J. Touwslager, Three-dimensional inhomogeneities in PEDOT:PSS films, J. Phys. Chem. B 108 (2004) 18820–18825.

[16] V. Shrotriya, G. Li, Y. Yao, C.-W. Chu, Y. Yang, Transition metal oxides as the buffer layer for polymer photovoltaic cells, Appl. Phys. Lett. 88 (2006) 0735081–0735083.

[17] M.D. Irwin, D.B. Buchholz, A.W. Hains, R.P.H. Chang, T.J. Marks, p-Type semiconducting nickel oxide as an efficiency-enhancing anode interfacial layer in polymer bulk-heterojunction solar cells, Proc. Nat. Acad. Sci 105 (2008) 2783–2787.

[18] U.K. Barik, S. Srinivasan, C.L. Nagendra, A. Subrahmanyam, Electrical and optical properties of reactive DC magnetron sputtered silver oxide thin films: role of oxygen, Thin Solid Films 429 (2003) 129–134.

[19] Q. Dong, Y. Zhou, J. Pei, Z. Liu, Y. Li, S. Yao, J. Zhang, W. Tian, All-spin-coating vacuum-free processed semi-transparent inverted polymer solar cells with PEDOT:PSS anode and PAH-D interfacial layer, Org. Electron. 11 (2010) 1327–1331.

[20] R.J. Kline, M.D. Mcgehee, M.F. Toney, Highly oriented crystals at the buried interface in polythiophene thin-film transistors, Nat. Mater. 5 (2006) 222–228.

[21] S.K. Hau, H.-L. Yip, O. Acton, N.S. Baek, H. Ma, A.K.-Y. Jen, Interfacial modification to improve inverted polymer solar cells, J. Mater. Chem. 18 (2008) 5113–5119.

[22] S.H. Brewer, D. Wicaksana, J.-P. Maria, A.I. Kingon, S. Franzen, Investigation of the electrical and optical properties of iridium oxide by reflectance FTIR spectroscopy and density functional theory calculations, Chem. Phys. 313 (2005) 25–31.

[23] K. Hong, K. Kim, J.-L. Lee, Enhancement of electrical property by oxygen doping to copper phtahalocyanine in inverted top emitting organic light emitting diodes, Appl. Phys. Lett. 95 (2009) 2133071–2133073.

[24] K. Hong, K. Kim, S. Kim, Y.H. Song, H.J. Kim, K.H. Song, K.C. Ahn, Y.-H. Tak, J.-L. Lee, In situ analysis of hole injection barrier of molybdenum-oxide-coated anode with organic materials using synchrotron radiation photoemission spectroscopy, J. Electrochem. Soc. 156 (2009) H648–H653.

[25] S.Y. Kim, K. Hong, H.W. Choi, K.Y. Kim, Y.-H. Tak, J.-L. Lee, Correlation between charge injection and charge balance in organic light emitting diodes using LiF and IrO_x interlayers, J. Electrochem. Soc. 156 (2009) J57–J61.

[26] M. Brinkmann, J.-C. Wittmann, Orientation of regioregular poly(3-hexylthiophene) by directional solidification: a simple method to reveal the semicrystalline structure of a conjugated polymer, Adv. Mater. 18 (2006) 860–863.

[27] D. Briggs, M.P. Seah, Practical Surface Analysis: Auger and X-Ray Photoelectron Spectroscopy, Vol. 1, John Wiley & Sons, New York, 1990.

[28] J.S. de Almeida, R. Ahuja, Electronic and optical properties of RuO_2 and IrO_2, Phys. Rev. B 73 (2006) 1651021–1651026.

[29] J. Backholm, G.A. Nikasson, Optical properties of electrochromic iridium oxide and iridium–tantalum oxide thin films in different coloration states, Sol. Energy Mater. Sol. Cells 92 (2008) 1388–1392.

[30] S.S.V. Bavel, M. Barenklau, G.D. with, H. Hoppe, J. Loos, P3HT/PCBM bulk heterojunction solar cells: impact of blend composition and 3D morphology on device performance, Adv. Funct. Mater. 20 (2010) 1458–1463.